Comparative transcription profiling of mRNA and lncRNA in pulmonary arterial hypertension after C75 treatment

Cuilan Hou
Shanghai Children's Hospital, Shanghai Jiaotong University
Lijian Xie
Shanghai Children's Hospital, Shanghai Jiaotong University
Tingxia Wang
Shanghai Children's Hospital, Shanghai Jiaotong University
Junmin zheng
Shanghai Children's Hospital, Shanghai Jiaotong University
Yuqi Zhao
The First Affiliated Hospital of Anhui Medical University
Qingzhu Qiu
Shanghai Children's Hospital, Shanghai Jiaotong University
Yi Yang
Zhejiang University School of Medicine
Tingting Xiao (ttxiao2017@163.com)
Shanghai Children's Hospital, Shanghai Jiaotong University

Research Article

Keywords: C75, Pulmonary arterial hypertension, High-throughput sequencing, Bioinformatic analyses, Cell cycle, Inflammatory

Posted Date: July 12th, 2022

DOI: https://doi.org/10.21203/rs.3.rs-1778632/v1

Additional Declarations: No competing interests reported.

Version of Record: A version of this preprint was published at BMC Pulmonary Medicine on January 31st, 2023. See the published version at https://doi.org/10.1186/s12890-023-02334-6.

Abstract

Objectives: To investigate mRNA and long non-coding RNA (lncRNA) expression profiles in monocrotaline (MCT)- mice.

Materials and Methods: Lung tissues (Control-Vehicle, MCT-Vehicle, and MCT-C75) were examined by high-throughput sequencing (HTS). Aberrantly expressed mRNAs and lncRNAs were analysed by bioinformatics. Cell proliferation and cell cycle analysis were performed to detect the potential protective effects of C75, an inhibitor of fatty acid synthase. The signal pathways associated with inflammatory responses were verified by RT-PCR.

Results: RNA sequencing data reveals 285 differentially expressed genes (DEGs) and 147 lncRNAs in the MCT-Vehicle group compared to the control group. After five-week of C75 treatment, 514 DEGs and 84 lncRNAs are aberrant compared to the MCT-Vehicle group. Analysis of DEGs and lncRNA target genes reveals that they were enriched in pathways related to cell cycle, cell division, and vascular smooth muscle contraction that contributes to the PAH pathological process. Subsequently, the expression of eight DEGs and three lncRNAs is verified using RT-PCR. Differentially expressed lncRNAs (ENSMUSG00000110393.2, Gm38850, ENSMUSG00000100465.1, ENSMUSG00000110399.1) may associate in PAH pathogenesis as suggested by co-expression network analysis. C75 can protect against MCT-induced PAH through its anti-inflammatory and anti-proliferation.

Conclusions: These DEGs and lncRNAs can be considered as novel candidate regulators of PAH pathogenesis. We propose that C75 treatment can partially reverse PAH pathogenesis through modulating cell cycle, cell proliferation, and anti-inflammatory.

Introduction

Pulmonary arterial hypertension (PAH) is a progressive and fatal disease characterized by increased pulmonary vascular resistance, which then leads to right ventricular failure and ultimately death[1, 2]. The incidence of PAH is about 1%, rising to 10% of people over 65 years old[3]. It is well known that many targeted therapeutics such as endothelin receptor antagonists, phosphodiesterase 5 inhibitors, and prostacyclin analogs, can improve the life quality of PAH patients[4, 5]. Despite the remarkable progress, patients with PAH still have a poor prognosis, and molecular pathways underlying the PAH pathogenesis are still remain largely unknown, thereby, it is urgent to discover novel therapeutic targets.

Over the past two decades, metabolic theory has become to be one of the most influential theories in PAH disease. For example, Gopinath group reported that metabolic remodeling occurred in the pulmonary arterial wall in PAH patients[6]. Paulin *et al.* proposed a metabolic theory that integrated cancer-like signals upstream and downstream of mitochondria, which could explain many characteristics of PAH vascular phenotypes, including proliferation and apoptosis resistance[7]. The PAH metabolic theory still needs further exploration. Singh *et al.* reported that the expression of fatty acid synthase (Fas) was increased in pulmonary artery smooth muscle cells (PASMCs) and lung tissues in PAH rats model[8]. They also pointed that Fas inhibition plays a protective role in regulating of PAH disease[8]. And our previous study also showed that Fas inhibition plays a key role in shielding PAH mice, and partially through the activation of PI3K/Akt signaling[9]. However, no comparative transcription profiling was performed after inhibition of Fas.

Non-coding RNAs are emerging as important regulatory molecules in the development of cardiopulmonary diseases including PAH. In 2010, the first report of investigating the global microRNA (miRNA) profiles of rat lungs during hypoxia and MCT-induced PAH showed that some miRNAs were specific and important in regulating the disease development[10]. Previously, we showed that several miRNAs (miRNA125-3p, miR-125-3p, miR-193, and miR-148-3p) were associated with PAH pathogenesis[11], our further data indicated that miR-29b targeted myeloid cell leukemia 1 and Cyclin D2 to regulate apoptosis and proliferation of PASMCs[12]. Interestingly, various lncRNAs such as Paxip1-as1 and Hoxaas3 are also associated with the regulation of PASMCs proliferation, migration, and apoptosis[13, 14].

Although some miRNAs or linRNAs were reported[11–14], but there still lack comprehensive understand of miRNA/lincRNA–mRNA in PAH. Thus we aimed to investigate potential mRNA and lncRNA expression profiles in PAH lung tissues using high-throughput sequencing (HTS) and explore the potential regulatory network in the pathogenesis of PAH.

Materials And Methods

Animals and experimental design

The animals were raised in the same way as our previously methods[9]. Twenty-one C57BL/6 mice (eight-week-old) were purchased from Shanghai Laboratory Animal Center (Shanghai, China), and grown under controlled conditions (45-55% relative humidity, 22 ± 2ºC and 12 h dark-light cycles), with unrestricted access to food and water. The health and weight of these mice were continuously monitored throughout the experimental period. The mice were randomly divided into three groups: 1) the disease group (n=8), in which mice received the MCT (60 mg/kg/week, Sigma, Germany) and vehicle (0.5%DMSO) for five weeks to induce PAH[15-18]; 2) the treatment group (n=8), in which MCT as described in the disease group, followed by C75 injection (2 mg/kg/week, dissolved in 0.5% DMSO) for five weeks[18]; and 3) the control group (n=8), which received an equivalent amount of vehicle (0.5%DMSO) each week.

Ethics approval

All methods (Animal experiments) were carried out in accordance with the Shanghai Jiaotong University Institutional Animal Care and Use Committee guidelines and regulations.

All methods in this manuscript are reported in accordance with ARRIVE guidelines (https://arriveguidelines.org) for the reporting of animal experiments.

Morphological and histological analyses

Mice lung slices, Hematoxylin-eosin (HE), and Masson staining were in the guide of our previously methods[19]. Mice lung tissues were excised, fixed at 10% formalin, and embedded in paraffin. According to the manufacturer's instructions, tissue sections (4 μm) were subjected to HE and Masson staining. HE staining was used for mice lung tissue pathological changes, while Masson staining was performed to evaluate the medial wall thickness in small pulmonary arteries. To assess the medial wall thickness[8], 20–25 muscular arteries, categorized as being 20–50 μm and 50–100 μm in diameter, from each lung were randomly outlined by an observer blinded to pharmacological treatment. The degree of medial wall thickness, presented as a ratio of medial area to cross-sectional area (media/CSA), was analyzed by using Image J.

Analysis of RVSP and right heart hypertrophy (RV/LV + S)

A left parasternal incision was made after mice were anesthetized. Then the ribs were partially resected, a 1.4-F microtip pressure transducer catheter (Millar Instruments) was carefully inserted into the right ventricular (RV), and Right ventricular systolic pressure (RVSP) was continuously monitored for 5 min using a PowerLab data acquisition system (AD Instruments)[20]. RV hypertrophy was evaluated in Fulton index measurements (weight of RV/LV + S), and it was determined according to the method described previously[21,22].

RNA extraction and high-throughput sequencing

RNA extraction and high-throughput sequencing was according previously methods[23]. RNAiso (Takara, Beijing, China) was utilized to extract total RNA from mice lung tissues. RNA integrity was evaluated by the Bio-analyzer 2100 system

(Agilent Technology, CA, USA). Ribosome RNA was isolated from 3 μg of RNA using a commercially available RNA Removal Kit (Epicentre, WI, USA). Thereafter, the sequencing library was constructed. PCR products were purified and library qualification was detected. The library was sequenced using the illumina Hiseq 3500 platform to generate 150 bps long paired-end reads. Raw and clean data were obtained after filtering for quality control. Reading counts for every sample were analysed using HTSeq v6.0. RPKM (reads per kilo base million mapped reads) and computed to estimate gene expression levels. The datasets generated and analysed during the current study are available in the [GEO data, Series GSE128358] repository.

Gene annotation and pathway identification

Gene Ontology (GO) was performed to determine the main functions of genes, lncRNAs, and their target genes. Biological pathways related to aberrantly expressed genes were analyzed based on KEGG database (http://www.genome.jp/kegg/). Benjamini-corrected $p < 0.05$ was used as the cut-off for significantly enriched biological processes.

Co-expression analysis of lncRNA and mRNA

Cis and trans assays were performed to reveal the relationship between the predicted targets of DEGs and lncRNAs. The interaction network of lncRNA-mRNA co-expression pairs (COR ≥ 0.7 and $p < 0.05$) was then constructed using Cytoscape 3.0. A lncRNA-miRNA regulatory network was established by Star Base v2.0 to determine the functions of candidate lncRNAs after C75 treatment. Six lncRNA sequences were obtained from NCBI (Supplementary Table 1). The MiRanda software (https://www.miranda.software/contact) was then used to predict the possible binding events between lncRNAs and miRNAs by accepting predicted scores that were above 140 and energy below -20.

CCK-8 and cell cycle assay

In vitro pulmonary hypertension was induced in pulmonary arterial smooth muscle cells (PASMCs) by incubating cells with hypoxia (3% O_2, 5% CO_2, 92% N_2) for 24 h. PASMCs were purchased from the Chinese Academy of Sciences Cell Bank (Shanghai) and cultured with Smooth Muscle Cell Medium (SMCM) (ScienCell, California, USA). Cell Counting Kit 8 (CCK-8) was used to detect PASMCs proliferation. And cells at passages 3–6 were used in experiments. Briefly, PASMCs were grown in a 96-well plate under hypoxia for 24 h and treated with or without C75 (50 μg/mL). Culture medium (SMCM) was deleted, 100 μL of SMCM and 10 μL CCK-8 detection solutions were added to each well of the 96-well plate. Background control composed of 100 μL SMCM and 10 μL CCK-8 was added. After incubating in a 37°C cell incubator for 2 h, the optical density of each well was read using a Thermo Scientific Microplate Reader (Thermo Fisher Scientific, USA) at 450 nm. The experiment was repeated at least three times. For cell cycle assay, the PAMSCs cells were pretreated as above, then the cells were collected and detected by flow cytometry. Each experiment was replicated at least three times.

Quantitative real-time polymerase chain (RT-PCR) reaction

RT-PCR was carried out to validate the HTS results using SYBR Green assays. Assays were performed with 2 μL of cDNA in 20 μL reactions. The cycling conditions were: 95°C for 10 min for initial denaturation and enzyme activation, followed by 40 cycles at 95°C for 15 s and 60°C for 1 min. All primers used in this study are shown in Table 2.

Statistical analyses

Differential expression analysis for any two groups was performed using the DESeq2 R package (1.26.0). A *P* value < 0.05 and fold Change ≥ 2 was set as the threshold for significantly differential expression. Student's *t*-test, one-way

ANOVA, and Pearson's correlation were performed using SPSS (version 22). *P*-values less than 0.05 were considered statistically significant.

Results

Morphological and pathological studies

The animal model dosing strategy is shown in Table 1. MCT injection induced pulmonary artery remodeling, while C75 (50 μg/kg/week) administration partially inhibited the ratio of vascular medial thickness of total vessel size (Figure 1A). Likewise, compared to the control, mice after MCT treatment showed significantly increased collagen content, and was partially reduced after C75 administration (Figure 1B). In line with the morphological change, we also observed a significant increase of both right ventricular systolic pressure (RVSP) and the ratio of the right ventricular wall weight to the left ventricular wall plus septum (RV/LV+S) following MCT injection. C75 reduced the increase of RVSP due to the MCT effect, but such effect was not significant in RV/LV+S (Figure 1C).

Characteristics of mRNAs and lncRNAs

The raw and clean data were submitted to the GEO repository (series record GSE128358). A total of 9,082 lncRNA transcripts were selected by intersecting coding potential calculator, coding non-coding index, and protein family database. These lncRNAs were classified into antisense lncRNAs (45.75%), bidirectional lncRNAs (1.65%), intergenic lncRNAs (41.75%), intrinsic sence lncRNAs (9.12%), overlapping sence lncRNAs (0.43%), and retained intron lncRNAs (1.3%) (Figure 1D). Compared to mRNAs, lncRNAs exhibited much lower transcript abundance (Figure 2A), higher tissue specificity (Figure 2B), and less conservative (Figure 2C). The lncRNAs identified are over 200 bps, containing more than 2 exomes (Figure 2D). These properties are consistent with lncRNA traits.

Profiles of mRNAs and lncRNAs

Volcano plots were plotted using gglot2 package to demonstrate gene/lncRNA expression based on RPKM among the three groups. Conservation analysis was performed and JS score was calculated. Correlations between mRNA and lncRNA profiles were significantly higher within groups than *inter-group correlations* (Figure 3A-B), suggesting that the results are highly reliable. Compared to the control group, 285 mRNAs (113 upregulated and 172 downregulated) and 147 lncRNAs (82 upregulated and 65 downregulated) were differentially expressed in the MCT-Vehicle group. Top 10 deregulated mRNAs and lncRNAs are presented in Tables 3-1 and 3-2, respectively. After five weeks of C75 treatment, 514 mRNAs (401 upregulated and 113 downregulated) and 84 lncRNAs (35 upregulated and 49 downregulated) were aberrantly expressed in the MCT-C75 group compared to the MCT-Vehicle group. The top 10 disordered mRNAs and lncRNAs are shown in Tables 4-1 and 4-2, respectively. Heat maps and volcano plots illustrate the expression profiles of mRNAs and lncRNAs after MCT and C75 treatment (Figure 3C-D). Venn diagram showed that only one mRNA, Hsd17b2, was decreased in the MCT-Vehicle group, but returned to normal level after C75 intervention (Figure 4A); not one lncRNA altered among them (Figure 4B). Aberrantly expressed mRNAs (Retnlg, Mmp8, S100a9, Ll1r2, S100a8, Slfn4, Ntrk2, and Ckap2) were selected and validated using RT-PCR assay (Figure 4C). Based on the RT-PCR results, six genes exhibited lower expression, while two genes exhibited higher expression in the MCT-Vehicle group. These effects were partially reversed by C75 treatment. These results of RT-PCR were consistent with the HTS (Figure 4D).

GO and KEGG analyses

Both GO and KEGG analyses were performed to explore the functions of aberrantly expressed mRNAs. Top 10 GO terms are illustrated in Figure 5. GO analysis revealed that up-regulated mRNAs between the MCT-Vehicle and control group were primarily associated with the cell cycle, microtubule-based movement, cell division, and mitotic nuclear division.

Down-regulated mRNAs were mainly associated with neutrophil chemotaxis, inflammatory response, and immune response (Figure 5A). Up-regulated mRNAs between the MCT-C75 and MCT-Vehicle were centered on fibrinolysis, hemostasis, and acute-phase response. Down-regulated mRNAs were involved in intracellular transport, cilium morphogenesis, cellular response to DNA damage stimulus, and actin filament polymerization (Figure 5A). KEGG analysis revealed that up-regulated mRNAs were mainly concentrated in the p53 signaling pathway, a PPAR signaling pathway, glycerophospholipid metabolism, pancreatic secretion, and metabolic pathways. Down-regulated mRNAs were involved with malaria, African trypanosomiasis, cytokine-cytokine receptor interaction, osteoclast differentiation, hematopoietic cell lineage, and cell adhesion molecules (Figure 5B). These results suggested that up-regulated mRNAs may directly promote PAH pathogenesis, while down-regulated mRNAs may suppress cell division and may indirectly contribute to PAH pathogenesis. GO and KEGG analysis indicated that the inflammatory response may play crucial roles in the PAH, we used RT-PCR assay to detect the pro-inflammation, anti-inflammation signal and metabolic pathways. Compared to the control group, the mRNA levels of TNF-α, IL-4, IL-5, IL6, IL-13 were increased. And C75 treatment can partially decrease TNF-α, IL-4, IL-5 (Figure 6A-E). PPAR-α mRNA level was increased in the MCT-treated mice, C75 treatment has little effect on the PPAR-α expression (Figure 6F).While PPAR-γ mRNA level was decreased in the MCT-treated mice, C75 treatment can increase the PPAR-γ expression (Figure 6G). We also detected Fas, CPT1, and GLUT mRNA levels, and found that C75 treatment can reverse the Fas increase (Figure 6H), reverse decreased GLUT mRNA (Figure 6I), and can partially reverse the CPT1 decrease induced by MCT (Figure 6J). The RT-PCR results indicated that inflammatory was activated in this PAH model, while C75 treatment can reverse the inflammatory partially.

Functional prediction of mRNAs regulated by aberrantly expressed cis- and trans-acting lncRNAs

GO analysis was performed to examine the function of mRNAs regulated by lncRNAs in cis and trans. Compared to the MCT-Vehicle group, aberrantly expressed lncRNA in C75-treated mice are shown in Figure 7. The mRNAs targeted in cis by aberrantly expressed lncRNAs are involved in multiple biological processes, such as cellular protein catabolic processes, modification-dependent protein catabolic processes, and macromolecule catabolic processes (Figure 7A). Disordered mRNAs targeted in trans by aberrantly expressed lncRNAs are associated with various biological processes, such as regulation of transcription, response to DNA damage stimulus, protein secretion, organelle fission, mitosis, cell cycle, and DNA repair (Figure 7B). Moreover, lncRNA-mRNA network analysis exhibited the possible relationship in trans (Figure 7C). Based on RT-PCR results, lncRNAs Gm41235 and Mirt2 exhibited lower expression in the MCT-Vehicle group compared to the control group. It was observed that the expression of lncRNAs Gm41235, Mirt2, and Gm38850 was partially rescued after C75 treatment (Figure 7D). And these RT-PCR results were consistent with the HTS (Figure 7E).

Co-expression networks

A comprehensive analysis of lncRNAs in lung tissues was carried out to understand the possible impacts of lncRNAs on PAH. A number of lncRNAs were aberrantly expressed after C75 treatment. A co-expression network (protein-coding genes and lncRNAs) was constructed to identify the potential functions and regulatory mechanisms of lncRNAs (Supplementary Figure 1).

Network of lncRNAs and miRNAs

It is known that lncRNAs and mRNAs have similar sequences and can be linked to a common miRNA. When lncRNAs bind to miRNA, upregulated lncRNAs act as competing endogenous RNAs, which prevent miRNAs from binding to untreated mRNA targets, thereby increasing their expression at post-transcriptional levels[24,25]. According to the predicted score of >140, and energy < −20, six lncRNAs and 1623 miRNAs that met these criteria were selected (Supplementary Table 2). Thereafter, 259 lncRNA-miRNA relationship pairs (at least five miRNA binding events), including six lncRNAs and 221miRNA (Supplementary Table 3) were filtered. The constructed lncRNA-miRNA network revealed the relationships between six abnormally expressed lncRNAs and 221 potential target miRNAs (Figure 8).

PASMC cell proliferation and cell cycle following C75 treatment

The PAMSCs cell proliferation ability was significantly increased under hypoxia condition, and its proliferation ability was decreased after incubation with C75 (50 μg/mL, 24 h) (Figure 9A). Fas mRNA expression was increased in hypoxia-induced, and C75 incubation could inhibit hypoxia-induced Fas increase (Figure 9B). Based on the flow cytometry assay, G1 phase duration was marginally reduced in hypoxia compared to that of control, whereas the ratio of S and G2 phase (S+G2) was increased. Incubation with 50 μg/mL of C75 for 24 h was able to restore the S and G2 phase (S+G2) ratio to that of the control group (Figure 9 C-F).

As MMP8 plays a crucial role in the PAH, and is widely expression in PAMSCs, we knochdown MMP8 in order to seek its role *in vitro*. We found that the MMP8 gene knockdown, it can inhibit hypoxia-induced PAMSCs cell proliferation (Figure 10A). We also found that MMP8 knockdown can inhibit hypoxia-induced inflammation, such as IL-6 and TNF-α expression (Figure 10 B-D).

Discussion

There are increasing evidences show that metabolic dysfunction underlies the PAH pathogenesis[6, 26], particularly altering lipid metabolism in PAH. However, there have been no studies on Fas transcription profiling in PAH. Utilizing HTS, we systematically demonstrated that both mRNAs and lncRNAs are abnormally expressed and altered in PAH after C75 treatment, and these DEGs and lncRNAs may provide novel candidate regulators for future molecular studies. Secondly, we found that C75 treatment can inhibit PASMCs cell cycle. We propose that C75 treatment can reverse PAH pathogenesis through regulating collagen contents, cell proliferation, cell cycle and anti-inflamtory, thus inhibition of FAS may serve as a potential means for reversing PAH.

Singh *et al.* first demonstrated that C75 treatment can reduce right ventricular pressure, pulmonary vascular remodeling, hypertrophy, and endothelial dysfunction in the lungs[8]. However, the expression patterns of DEGs and lncRNAs after C75 treatment in PAH animal model have not been comprehensively studied. HTS technology allows us to discover previously inaccessible complexities of transcription, such as novel promoters and isoforms. Thus, this study takes the initiative to describe DEGs and lncRNAs to further our understanding of mRNAs and lncRNAs that are associated with PAH pathogenesis, and some of the typical genes were confirmed by RT-PCR. It was reported that dysfunction of collagen digestion enzymes (MMP2 and MMP8), and TIMP1 (a collagenase inhibitor) were associated with pulmonary fibrosis[27]. Loss of the peroxisome proliferator-activated receptor γ (PPARγ) was associated with PASMC proliferation and pulmonary arterial remodeling[28]. In this study, we found that C75 treatment can partially decrease TNF-α, IL-4, IL-5 mRNA levels (Fig. 6A-E). We also found that the PPAR-α mRNA level was increased in the MCT-treated mice, and C75 treatment can partially reverse (Fig. 6F). C75 had an opposite role in regulating the PPAR-γ expression (Fig. 6G). The RT-PCR results indicated that inflammatory is activated in this PAH model, while C75 treatment can partially reverse the inflammatory response.

LncRNAs are a part of endogenous RNAs that act as gene expression regulators and are involved in various developmental and physiological processes and diseases[29, 30]. Analyzing the expression profiles of mRNAs and lncRNA offers new insights into PAH pathogenesis and pathophysiology, and the possible effects of C75 treatment. Pulmonary vascular remodeling including pulmonary vasculature thickening, is a major characteristic of PAH[22]. Previous studies exhibited that pulmonary vascular remodeling coupled with an increase in RVP leads to RVH, and right ventricular heart failure[31]. In this study, we found that C75 can partially attended MCT-induced PAH mice pulmonary vascular remodeling (Fig. 1), and our previous study also showed that C75 has a protective in right ventricular function in hypoxia-induced PAH mice[9], suggesting that inhibition of Fas plays a protective role in PAH.

Cis and trans methods were employed to detect the potential functions of lncRNAs. The cis-acting lncRNA acts on its neighboring genes on the same allele. GO and KEGG analyses of these protein-coding genes showed that these genes mainly belongs to cellular protein catabolic processes, modification-dependent protein catabolic processes, and macromolecule catabolic processes (Fig. 7A). The mRNAs targeted in trans by abnormally expressed lncRNAs are involved in various biological processes, such as transcription, regulation of transcription, response to DNA damage stimulus, protein secretion, organelle fission, mitosis, cell cycle, and DNA repair (Fig. 7B). As for the switch of glycolytic phenotype, we detected GLUT mRNA levels, and C75 treatment can partially reverse decreased GLUT mRNA induced by MCT (Fig. 6I). Paula Mera *et al.* reported that C75 is a potent inhibitor of CPT1, the rate-limiting step in fatty-acid oxidation both *in vitro* and *in vivo*[32]. We also detected Fas and CPT1 mRNA levels, we found that C75 treatment can reverse the Fas increase (Fig. 6H), and partially reverse the CPT1 decrease induced by MCT (Fig. 6J). As C75 can alter glycolytic phenotype and fatty-acid oxidation, we propose that these findings fit into the current paradigm of metabolic theory of PAH. Expression of six lncRNAs and 1623 miRNAs is altered significantly after C75 treatment, suggesting the existence of relationships between the six aberrantly expressed lncRNAs and its 221 potential target miRNAs within the lncRNA-miRNA network.

Conclusions

Altogether, we performed a comprehensive study of miRNA/lncRNA-mRNA in PAH lung tissues after C75 treatment. We identified some dysregulated mRNAs and lncRNAs which may be potential drivers as well as diagnostic and therapeutic biomarkers of PAH (the dysregulated mRNAs and lncRNAs sample sizes are still needed to expand for validation). GO and KEGG pathway analysis reveals these targets are related to cell cycle, cell division, and vascular smooth muscle contraction that contributes to the pathological process. Differentially expressed lncRNAs such as ENSMUSG00000110393.2, Gm38850, ENSMUSG00000085532.1, ENSMUSG00000100465.1, ENSMUSG00000110399.1, may be associate with the relieve of PAH. We propose that these lncRNA and DEGs may be promising candidates for molecular regulators of PAH pathogenesis.

Declarations

Ethics approval and consent to participate

The animal experiments were approved by the Shanghai Jiaotong University Institutional Animal Care and Use Committee. All methods (Animal experiments) were carried out in accordance with the Shanghai Jiaotong University Institutional Animal Care and Use Committee guidelines and regulations. All methods in this manuscript are reported in accordance with ARRIVE guidelines (https://arriveguidelines.org) for the reporting of animal experiments.

Consent for publication

Not applicable.

Availability of data and materials

The datasets generated and analysed during the current study are available in the [GEO data, Series GSE128358] repository (https://www.ncbi.nlm.nih.gov/geo/query/acc.cgi?acc=GSE128358). The data used to support the findings in this study are available from the corresponding author upon request.

Competing interests

The authors declare that they have no competing interests.

Funding

This work is sponsored by National Natural Science Foundation of China (NSFC) (no. 81900437, 82170518), the Interdisciplinary Program of Shanghai Jiao Tong University (YG2021ZD26), and Shanghai Children's hospital (2019YQ06, 2020YGZQ10). No benefits in any form were received from a commercial organization directly or indirectly.

Authors' Contributions

Tingting Xiao and Cuilan Hou designed the project. Cuilan Hou operated the project and wrote the manuscript with the input of Lijian Xie and Yuqi Zhao. Tingxia Wang, Junmin zheng, Qingzhu Qiu, and Yi Yang analyzed most of the date. All authors read and approved the final manuscript.

Acknowledgements

We thanks the above funds for their support and the team work of all authors.

References

1. Bai Y, Li ZX, Wang HL, Lian GC, Wang Y. The protective effects of PCPA against monocrotaline-induced pulmonary arterial hypertension are mediated through the downregulation of NFAT-1 and NF-kappaB. *INT J MOL MED*, 40(1), 155-163 (2017).
2. Chen YC, Yuan TY, Zhang HF *et al.*. Salvianolic acid A attenuates vascular remodeling in a pulmonary arterial hypertension rat model. *ACTA PHARMACOL SIN*, 37(6), 772-782 (2016).
3. Hoeper MM, Humbert M, Souza R *et al.*. A global view of pulmonary hypertension. *Lancet Respir Med*, 4(4), 306-322 (2016).
4. Bubb KJ, Trinder SL, Baliga RS *et al.*. Inhibition of phosphodiesterase 2 augments cGMP and cAMP signaling to ameliorate pulmonary hypertension. *CIRCULATION*, 130(6), 496-507 (2014).
5. Coons JC, Pogue K, Kolodziej AR, Hirsch GA, George MP. Pulmonary Arterial Hypertension: a Pharmacotherapeutic Update. *CURR CARDIOL REP*, 21(11), 141 (2019).
6. Sutendra G, Bonnet S, Rochefort G *et al.*. Fatty acid oxidation and malonyl-CoA decarboxylase in the vascular remodeling of pulmonary hypertension. *SCI TRANSL MED*, 2(44), 44r-58r (2010).
7. Paulin R, Michelakis ED. The metabolic theory of pulmonary arterial hypertension. *CIRC RES*, 115(1), 148-164 (2014).
8. Singh N, Manhas A, Kaur G, Jagavelu K, Hanif K. Inhibition of fatty acid synthase is protective in pulmonary hypertension. *Br J Pharmacol*, 173(12), 2030-2045 (2016).
9. Hou C, Chen J, Zhao Y *et al.*. The Emerging Role of Fatty Acid Synthase in Hypoxia-Induced Pulmonary Hypertensive Mouse Energy Metabolism. *OXID MED CELL LONGEV*, 2021, 9990794 (2021).
10. Caruso P, MacLean MR, Khanin R *et al.*. Dynamic changes in lung microRNA profiles during the development of pulmonary hypertension due to chronic hypoxia and monocrotaline. *Arterioscler Thromb Vasc Biol*, 30(4), 716-723 (2010).
11. Xiao T, Xie L, Huang M, Shen J. Differential expression of microRNA in the lungs of rats with pulmonary arterial hypertension. *MOL MED REP*, 15(2), 591-596 (2017).
12. Chen J, Li Y, Li Y *et al.*. Effect of miR-29b on the Proliferation and Apoptosis of Pulmonary Artery Smooth Muscle Cells by Targeting Mcl-1 and CCND2. *BIOMED RES INT*, 2018, 6051407 (2018).
13. Jandl K, Thekkekara PH, Marsh LM *et al.*. Long non-coding RNAs influence the transcriptome in pulmonary arterial hypertension: the role of PAXIP1-AS1. *J PATHOL*, (2018).

14. Zhang CY, Liu M, Wan JM *et al.*. Role of Noncoding RNA in Pulmonary Arterial Hypertension and Potential Drug Therapeutic Target. *CURR TOP MED CHEM*, 18(12), 975-986 (2018).
15. Goto J, Ishikawa K, Kawamura K *et al.*. Heme oxygenase-1 reduces murine monocrotaline-induced pulmonary inflammatory responses and resultant right ventricular overload. *Antioxid Redox Signal*, 4(4), 563-568 (2002).
16. Bowen TS, Adams V, Werner S *et al.*. Small-molecule inhibition of MuRF1 attenuates skeletal muscle atrophy and dysfunction in cardiac cachexia. *J Cachexia Sarcopenia Muscle*, 8(6), 939-953 (2017).
17. Egan PC, Liang OD, Goldberg LR *et al.*. Low dose 100 cGy irradiation as a potential therapy for pulmonary hypertension. *J CELL PHYSIOL*, 234(11), 21193-21198 (2019).
18. Gabrielson EW, Pinn ML, Testa JR, Kuhajda FP. Increased fatty acid synthase is a therapeutic target in mesothelioma. *CLIN CANCER RES*, 7(1), 153-157 (2001).
19. Hou CL, Wang MJ, Sun C *et al.*. Protective Effects of Hydrogen Sulfide in the Ageing Kidney. *OXID MED CELL LONGEV*, 2016, 7570489 (2016).
20. Chen G, Zuo S, Tang J *et al.*. Inhibition of CRTH2-mediated Th2 activation attenuates pulmonary hypertension in mice. *J EXP MED*, 215(8), 2175-2195 (2018).
21. Kaur G, Singh N, Lingeshwar P, Siddiqui HH, Hanif K. Poly (ADP-ribose) polymerase-1: an emerging target in right ventricle dysfunction associated with pulmonary hypertension. *PULM PHARMACOL THER*, 30, 66-79 (2015).
22. Kaur G, Singh N, Samuel SS *et al.*. Withania somnifera shows a protective effect in monocrotaline-induced pulmonary hypertension. *PHARM BIOL*, 53(1), 147-157 (2015).
23. Wang W, Li J, Zhang Z *et al.*. Genome-wide analysis of acute traumatic spinal cord injury-related RNA expression profiles and uncovering of a regulatory axis in spinal fibrotic scars. *Cell Prolif*, 54(1), e12951 (2021).
24. Ge D, Han L, Huang S *et al.*. Identification of a novel MTOR activator and discovery of a competing endogenous RNA regulating autophagy in vascular endothelial cells. *AUTOPHAGY*, 10(6), 957-971 (2014).
25. Ma MZ, Chu BF, Zhang Y *et al.*. Long non-coding RNA CCAT1 promotes gallbladder cancer development via negative modulation of miRNA-218-5p. *CELL DEATH DIS*, 6, e1583 (2015).
26. Dromparis P, Michelakis ED. Mitochondria in vascular health and disease. *ANNU REV PHYSIOL*, 75, 95-126 (2013).
27. Ovet H, Oztay F. The copper chelator tetrathiomolybdate regressed bleomycin-induced pulmonary fibrosis in mice, by reducing lysyl oxidase expressions. *BIOL TRACE ELEM RES*, 162(1-3), 189-199 (2014).
28. Xie X, Li S, Zhu Y *et al.*. Egr-1 mediates leptin-induced PPARgamma reduction and proliferation of pulmonary artery smooth muscle cells. *MOL BIOL CELL*, 29(3), 356-362 (2018).
29. Dey BK, Mueller AC, Dutta A. Long non-coding RNAs as emerging regulators of differentiation, development, and disease. *Transcription*, 5(4), e944014 (2014).
30. Knoll M, Lodish HF, Sun L. Long non-coding RNAs as regulators of the endocrine system. *NAT REV ENDOCRINOL*, 11(3), 151-160 (2015).
31. Dimauro I, Pearson T, Caporossi D, Jackson MJ. A simple protocol for the subcellular fractionation of skeletal muscle cells and tissue. *BMC Res Notes*, 5, 513 (2012).
32. Mera P, Bentebibel A, Lopez-Vinas E *et al.*. C75 is converted to C75-CoA in the hypothalamus, where it inhibits carnitine palmitoyltransferase 1 and decreases food intake and body weight. *BIOCHEM PHARMACOL*, 77(6), 1084-1095 (2009).

Tables

Table 1. The animal model method was showed in the following table.

Groups	Week 1	Week 2	Week 3	Week 4	Week 5
Control-Vehicle	Vehicle + Vehicle	Vehicle	Vehicle	Vehicle	Vehicle
MCT-Vehicle	MCT+Vehicle	Vehicle	Vehicle	Vehicle	Vehicle
MCT-C75	MCT+C75	C75	C75	C75	C75

Table 2. All primers used in this study are shown in the following Table.

Primer	Forward sequence	Reverse sequence
Retnlg	TGTCACTGGTTGTGCTTGTG	CCCAGTCCATTGTTGAGCAC
Mmp8	ACGCACCCTATGAGGACAAA	TGGCTGGGAATGCCAGATTA
S100a9	GCCAACAAAGCACCTTCTCA	TGTCAGGGTGTCCTTCCTTC
Ll1r2	TGGTGCGGACAATGTTCATC	ACGCACCCTATGAGGACAAA
S100a8	TTCGAGGAGTTCCTTGCGAT	AGCTCTGCTACTCCTTGTGG
Slfn4	AAGAGCTGGGCTTTGGATCT	GCGCCTAGTTTCCCAAGAAG
Ntrk2	ACACGAAACAAGCTGACGAG	CGGATTACCCGTCAGGATCA
Ckap2	TACACCTCGGCTGCAAAGTA	GGCAGTCGTGAAGTCTTGTC
Gm38850	CTTCCTGTATCGCCCAGGAT	CATAAATTGGGCGTGGCTGA
Gm41235	TGGATGTCACACCTGATGCT	TTGTGTGATGCCCAAACCTG
Mirt2	TGCGCTACCATCTTTGAACG	AACAGTGAGGGAGGAATGGG
GAPDH	GTCGGTGTGAACGGATTTGG	TGATGGGCTTCCCGTTGATG

Table 3-1.Top 10 up-regulated and down-regulated lncRNAs (MCT-Vehicle vs. Control-Vehicle)

Symbol	Chromosomal Position	Control-Vehicle normalize	MCT-Vehicle normalize	log_2 FC	p-value	Up/Down
ENSMUSG00000112441.1	chr12:8291024-8293694	3	32	3.2915026	0.0030079	up
ENSMUSG00000107605.1	chr6:90459711-90461468	4	27.5	2.7232757	0.0040755	up
ENSMUSG00000112647.1	chr10:98653799-98699710	7	37.5	2.3810823	0.0192184	up
ENSMUSG00000109957.1	chr8:122339171-122343100	3	26.5	2.9411917	0.0240806	up
ENSMUSG00000114105.1	chr12:25300071-25304613	4	21.5	2.3530836	0.0246912	up
ENSMUSG00000110290.1	chr8:92465767-92469665	4.5	27	2.6516029	0.0311117	up
ENSMUSG00000097219.1	chr11:51949882-52269514	40	127.5	1.4952014	0.035351	up
ENSMUSG00000098001.1	chr8:80933534-80938667	8	34	2.0443405	0.0353627	up
Vaultrc5	chr18:36801763-36802107	248.5	683.5	1.4588887	1.41E-06	up
LOC105246895	chr11:120235184-120239123	10.5	66	2.6002823	5.38E-05	up
Gm40799	chr10:127107362-127113573	2.5	41.5	3.9511874	7.10E-05	up
ENSMUSG00000097554.1	chr5:5781530-5783636	225.5	79	-1.4568222	0.0072437	down
ENSMUSG00000111250.1	chr9:77836030-77848111	33	9.5	-1.8350256	0.016356	down
ENSMUSG00000107736.1	chr6:121255203-121272685	69	30	-1.2331487	0.0164294	down
ENSMUSG00000097576.1	chr16:38451982-38453493	42	7.5	-2.5782671	0.0192785	down
ENSMUSG00000087340.1	chrX:167164097-167171278	18.5	3	-2.7450978	0.0355979	down
ENSMUSG00000103170.1	chr3:52198248-52200489	28.5	7.5	-1.8897878	0.0411948	down
Gm41235	chr14:103043478-103048082	348.5	53	-2.8783353	3.65E-07	down
1600010M07Rik	chr7:109998377-110006646	100.5	29	-1.8322912	7.38E-05	down
Gm30286	chr2:131014185-131025161	379.5	84.5	-2.105982	0.0002835	down
Gm13605	chr2:35223695-35254166	31	2	-3.9802018	0.0003077	down

Table 3-2. Top 10 up-regulated and down-regulated lncRNAs (MCT-C75 vs. MCT-Vehicle)

Symbol	Chromosomal Position	MCT-Vehicle normalize	MCT-C75 normalize	log_2 FC	p-value	Up/Down
ENSMUSG00000102196.1	chr2:11315372-11319874	21	103	2.3662741	3.45E-06	up
ENSMUSG00000100465.1	chr5:149234816-149247682	1.5	47.5	5.0271267	4.48E-06	up
ENSMUSG00000087340.1	chrX:167164097-167171278	3	34	3.5396281	0.0011068	up
ENSMUSG00000108197.1	chr6:86687823-86688428	0.5	18.5	5.2597749	0.0031102	up
ENSMUSG00000085532.1	chr11:63173914-63188454	12	43.5	1.9194104	0.0040397	up
ENSMUSG00000108308.1	chr6:91599232-91605514	4.5	25	2.5651125	0.0165033	up
ENSMUSG00000105560.1	chr5:4784753-4799094	11.5	36	1.7164354	0.019711	up
ENSMUSG00000105699.1	chr5:140605789-140606551	3.5	19	2.4695539	0.0491302	up
Gm41235	chr14:103043478-103048082	53	359	2.8386814	1.35E-12	up
Gm38850	chr6:86653954-86663064	888	2212.5	1.3850536	1.47E-12	up
ENSMUSG00000110399.1	chr8:25443668-25454107	21.5	2	-3.3533301	0.0058612	down
ENSMUSG00000107689.1	chr6:86513891-86516273	19	2	-3.1682999	0.0127772	down
ENSMUSG00000110393.2	chr13:65241753-65250154	142	62	-1.1271112	0.0132598	down
ENSMUSG00000109028.1	chr7:70548869-70554924	40.5	10	-1.9304727	0.0185882	down
ENSMUSG00000098061.1	chr12:109640341-109642351	47.5	12.5	-1.9088353	0.0276344	down
ENSMUSG00000096983.1	chr11:88039578-88047360	32	9	-1.7770616	0.0306435	down
ENSMUSG00000096984.1	chr1:163301790-163303620	22.5	3	-2.8080874	0.0323113	down
ENSMUSG00000112433.1	chr10:78248880-78256111	20.5	3	-2.6735213	0.0334734	down
ENSMUSG00000111868.1	chr10:44851393-44866786	20	4.5	-2.0949938	0.0376827	down
ENSMUSG00000085411.1	chr2:167858585-167862542	28	6	-2.173601	0.0388288	down

Table 4-1. Top 10 up-regulated and down-regulated mRNAs (MCT-Vehicle vs. Control-Vehicle)

Symbol	Chromosomal Position	Control-Vehicle normalize	MCT-Vehicle normalize	$\log_2$ FC	p-value	Up/Down
Ttn	chr2:76703980-76982557	8935	22213.5	1.2427283	1.89E-10	up
Ntrk2	chr13:58806569-59133970	390	860.5	1.0885439	1.31E-08	up
Kcnc3	chr7:44590661-44604751	435	916.5	1.0262368	1.32E-08	up
Ckap2	chr8:22168149-22185819	147.5	484.5	1.7217981	4.14E-07	up
Iqgap3	chr3:88082051-88121048	215	581	1.4181361	1.39E-06	up
Gtse1	chr15:85859690-85876573	30.5	150.5	2.3038095	8.95E-06	up
Npas2	chr1:39193715-39363240	365	808	1.0730423	4.26E-05	up
Gm9780	chr14:26027782-26042963	66.5	214.5	1.6404044	5.19E-05	up
Chsy3	chr18:59175340-59411336	160.5	356	1.1008269	7.13E-05	up
Wisp1	chr15:66891325-66923205	86.5	239	1.3969618	0.0001027	up
S100a9	chr3:90692630-90695721	9514.5	1805	-2.4365459	2.38E-95	down
S100a8	chr3:90669071-90670034	8895	1695.5	-2.4247112	4.61E-85	down
Slfn4	chr11:83175172-83190216	6051.5	1077.5	-2.5706601	5.37E-30	down
Mmp8	chr9:7558429-7568486	3691.5	850.5	-2.1926784	1.38E-28	down
Retnlg	chr16:48872608-48874498	1614.5	460.5	-1.8714284	3.38E-25	down
Dhrs9	chr2:69380462-69403086	981.5	177.5	-2.5533365	9.77E-21	down
Ccr1	chr9:123962126-123968692	2904	1032.5	-1.5605265	9.39E-18	down
Slc2a3	chr6:122727809-122802274	2285	947	-1.3191384	9.23E-17	down
Sirpb1b	chr3:15495754-15575067	811.5	233.5	-1.8636476	9.84E-16	down
Clec4e	chr6:123281789-123289871	1141.5	209.5	-2.5408385	1.18E-15	down

Table 4-2.Top 10 up-regulated and down-regulated mRNAs (MCT-C75 vs. MCT-Vehicle)

Symbol	Chromosomal Position	MCT-Vehicle normalize	MCT-C75 normalize	log_2 FC	p-value	Up/Down
Il1r2	chr1:40083308-40125230	545	2848.5	2.4452348	3.97E-84	up
Mmp8	chr9:7558429-7568486	850.5	4327.5	2.4055314	2.67E-74	up
Retnlg	chr16:48872608-48874498	460.5	1990	2.1717867	3.98E-56	up
Clec4d	chr6:123262107-123275268	355	1639.5	2.262501	1.62E-37	up
Slfn4	chr11:83175172-83190216	1077.5	5131.5	2.3228931	8.67E-34	up
Fgg	chr3:83007724-83015056	911.5	2932.5	1.7434494	2.83E-27	up
H2-Q10	chr17:35470089-35474563	303	1125.5	1.9528828	1.04E-26	up
Serpina1e	chr12:103946931-103956897	1536	3686	1.317478	8.71E-26	up
Fgb	chr3:83042246-83049863	759	2608	1.8304191	3.37E-24	up
Clec4e	chr6:123281789-123289871	209.5	992	2.2964289	5.01E-24	up
Slc7a10	chr7:35186352-35201116	1140	512	-1.089346	6.39E-09	down
Npas2	chr1:39193715-39363240	808	296.5	-1.3756141	1.05E-08	down
Hcn1	chr13:117602320-117981028	67.5	15	-2.1064787	0.0002332	down
Sbspon	chr1:15853862-15892722	258	103.5	-1.2465895	0.0004178	down
A730017C20Rik	chr18:59062181-59076962	27.5	1	-4.7317615	0.0005319	down
M1ap	chr6:82946908-83030309	100	33.5	-1.5235042	0.0005978	down
Kctd19	chr8:105382807-105413502	53	12.5	-2.0154139	0.0016237	down
Zfp239	chr6:117863077-117872766	67	19	-1.7555554	0.0017625	down
Trpm3	chr19:22137798-22989897	75.5	25	-1.5348774	0.0021623	down
Sycp1	chr3:102818499-102936100	70	20.5	-1.7157192	0.0021941	down

Figures

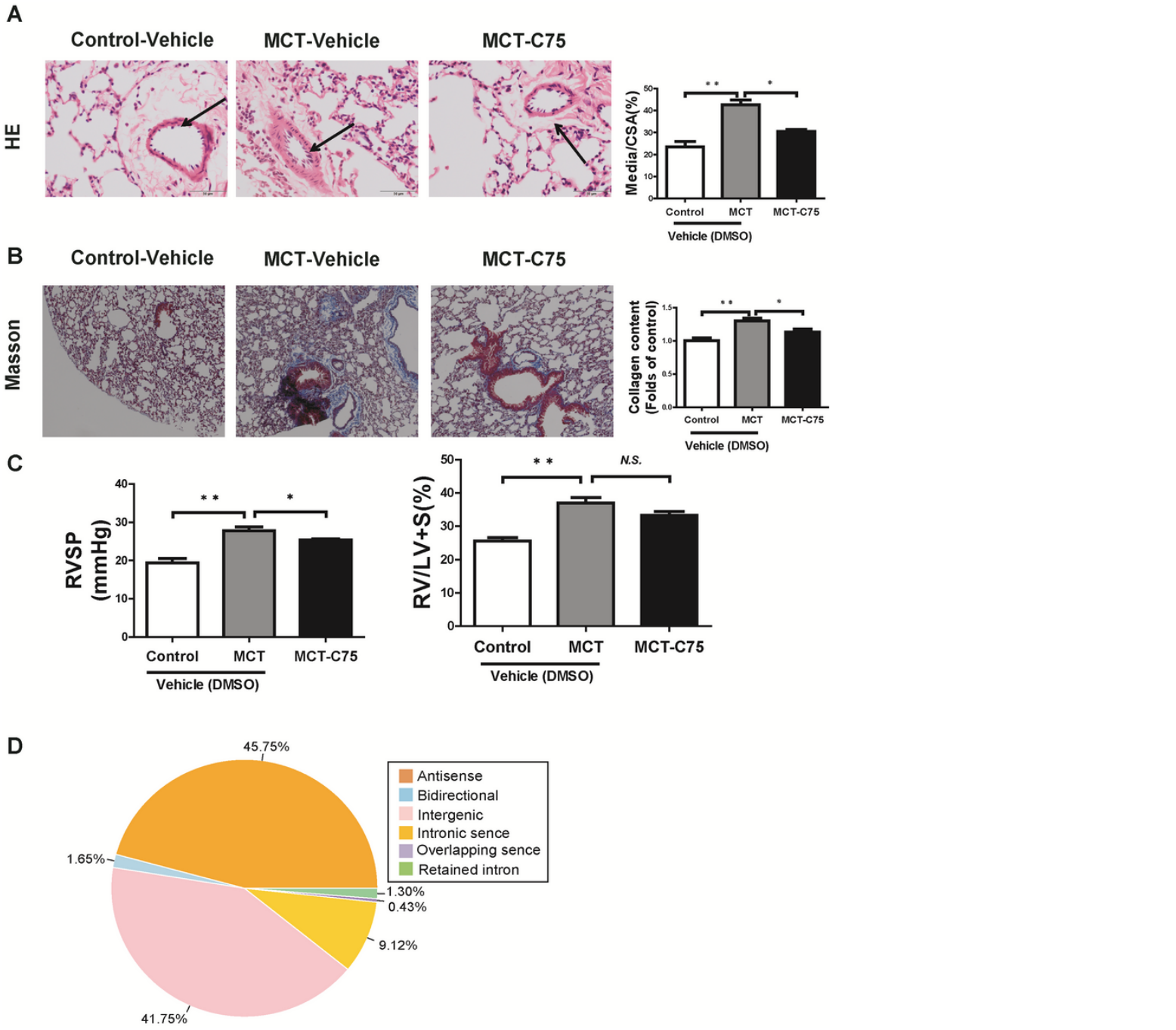

Figure 1

HE and Masson staining of lung tissues of MCT -induced PAH mice. Scale bars = 50 μm. A. Representative graphs of HE staining and quantification of the ratio of vascular medial thickness of total vessel size (Media/cross-sectional area [CSA]) for the PAH model. B. Representative graphs of Masson staining and collagen contents statistics. C. RVSP and ratio of RV/LV+S in mice after exposure to monocrotaline. D. These lncRNAs were classified into antisense lncRNAs, bidirectional lncRNAs, intergenic lncRNAs, intrinsic sence lncRNAs, overlapping sence lncRNAs, and retained intron lncRNAs. Right ventricular systolic pressure (RVSP); Hematoxylin-eosin (HE); Monocrotaline (MCT).

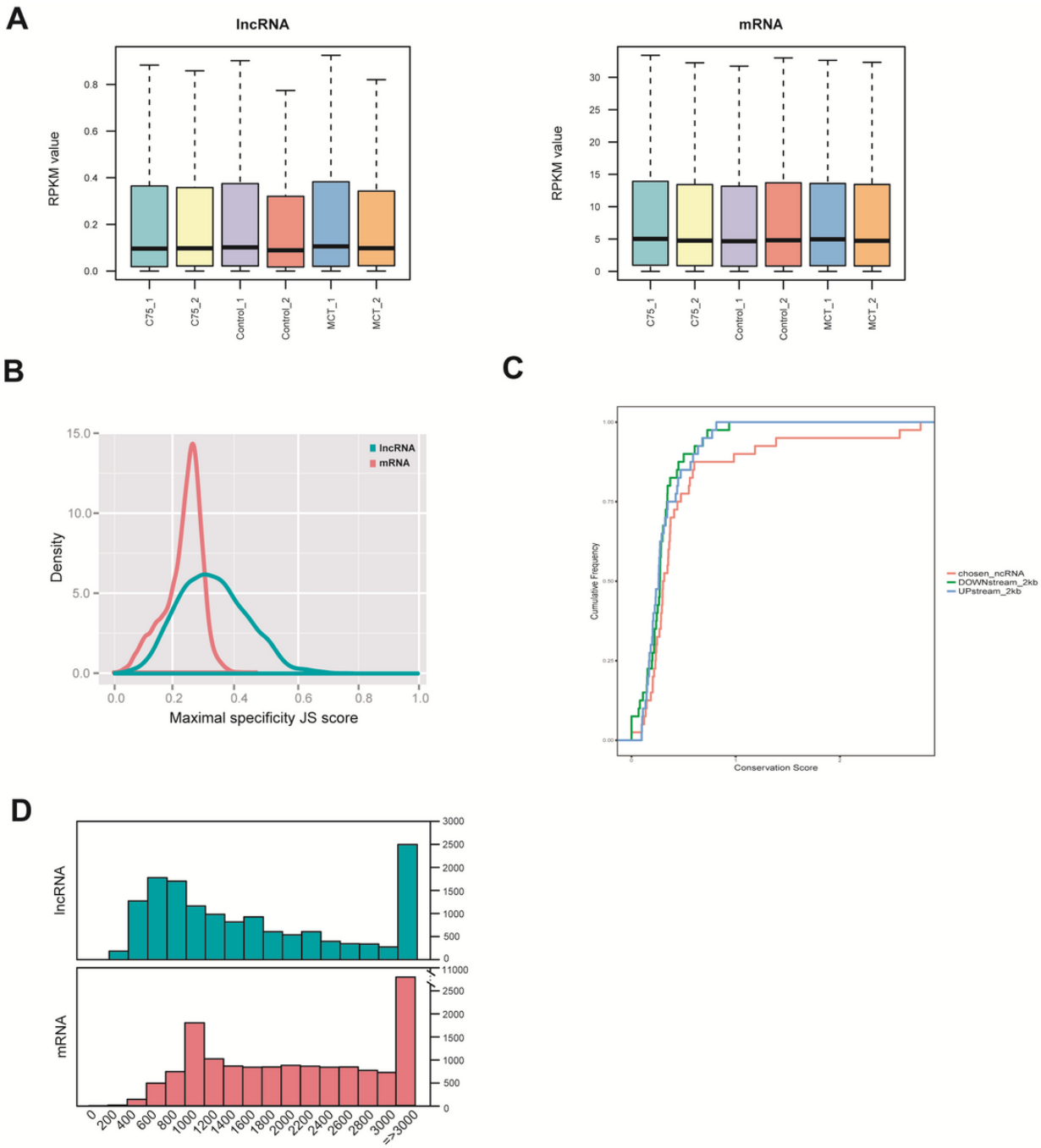

Figure 2

Comparison of mRNA and lncRNA characteristics. A. RPKM distribution of mRNAs and lncRNAs. B. JS score distribution of mRNAs and lncRNAs. C. Conservation scores for two individual subtypes of mRNAs and lncRNAs. D. Transcript lengths of mRNAs and lncRNAs.

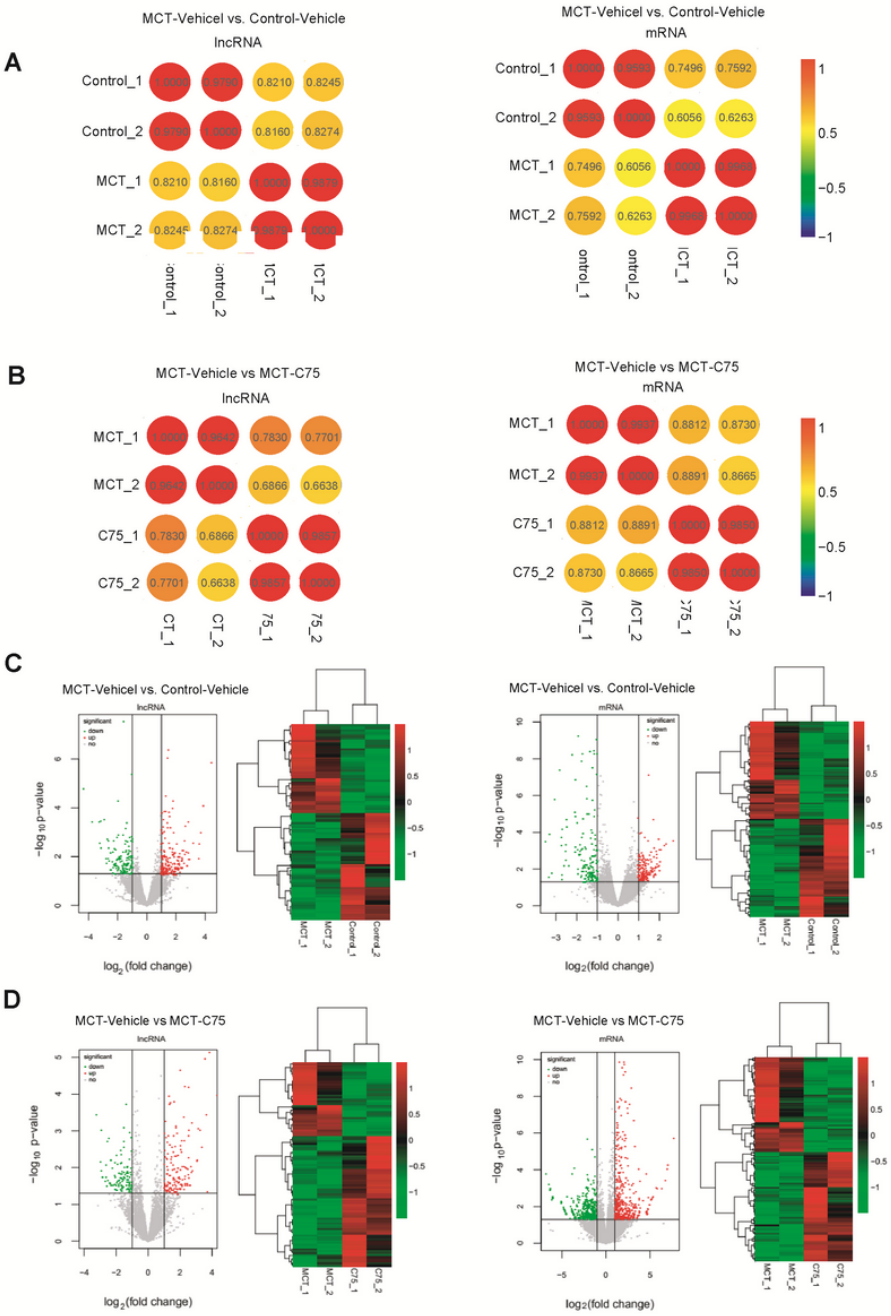

Figure 3

Aberrantly expressed genes in two-two comparison samples. A. The possible correlation between aberrantly expressed lncRNA profiles among the three groups: MCT-Vehicle Vs Control-Vehicle, MCT-Vehicle Vs MCT-C75. B. The possible correlation between aberrantly expressed mRNA profiles among the three groups: MCT-Vehicle Vs Control-Vehicle, MCT-Vehicle Vs MCT-C75. C-D. Volcano plot and hierarchically clustered heat map illustrating differentially expressed lncRNAs and miRNAs among the three groups: MCT-Vehicle Vs Control-Vehicle, MCT-Vehicle Vs MCT-C75. Upregulated mRNAs are shown in red while downregulated mRNAs are shown in green (fold change ≥ 2 and $p \leq 0.05$).

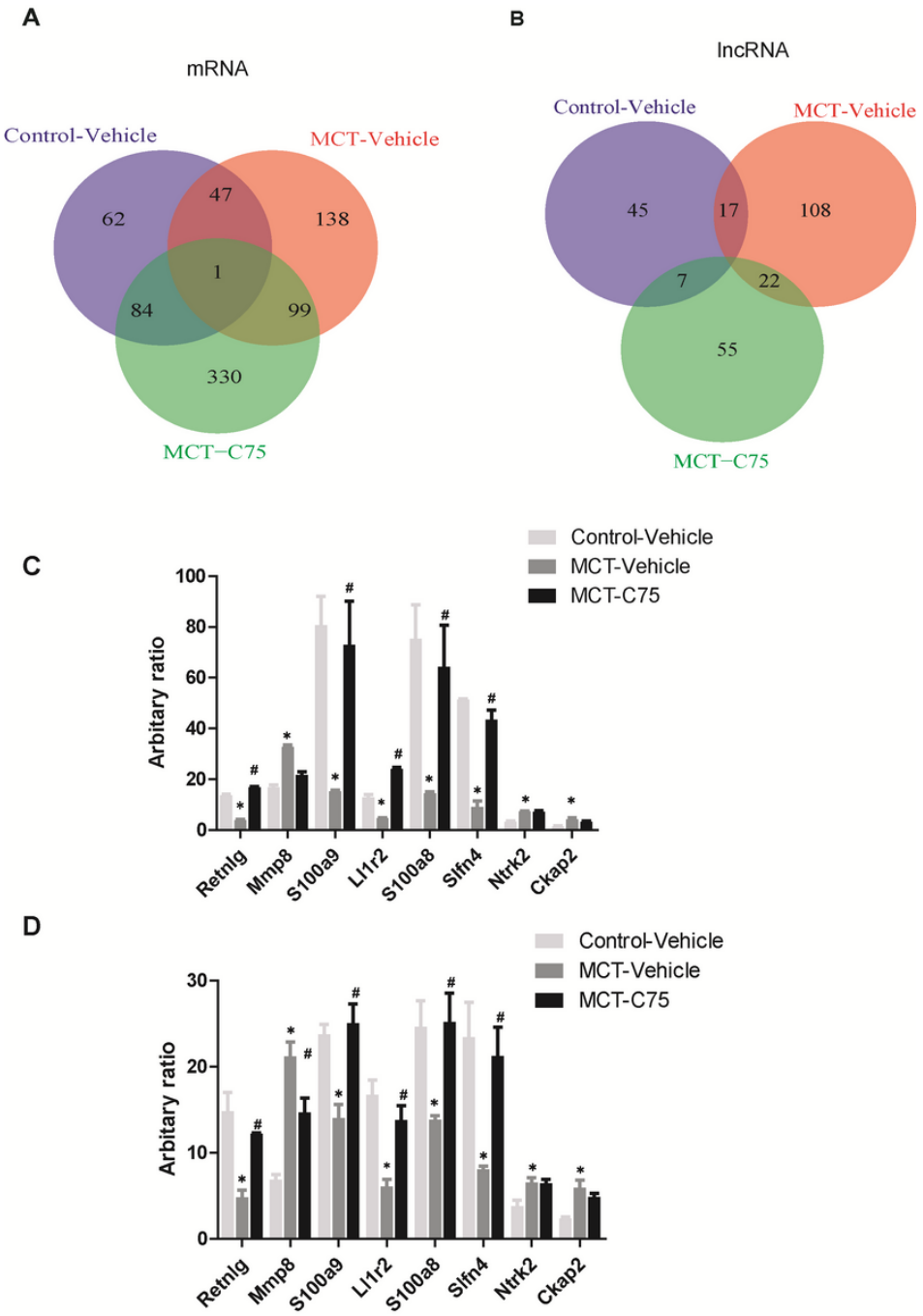

Figure 4

Venn diagram analysis and RT-PCR validation of these dysregulated mRNAs. A. Venn diagram of mRNAs among the three groups and only one of the mRNAs Hsd17b2 was decreased in the MCT-Vehicle group, but return to normal level after C75 intervention. B. Venn diagram of lncRNAs among the three groups and not one lncRNA altered among them. C. RT-PCR validation of dysregulated mRNAs. D. Dysregulated mRNAs after the HTS analysis. *$p < 0.05$.

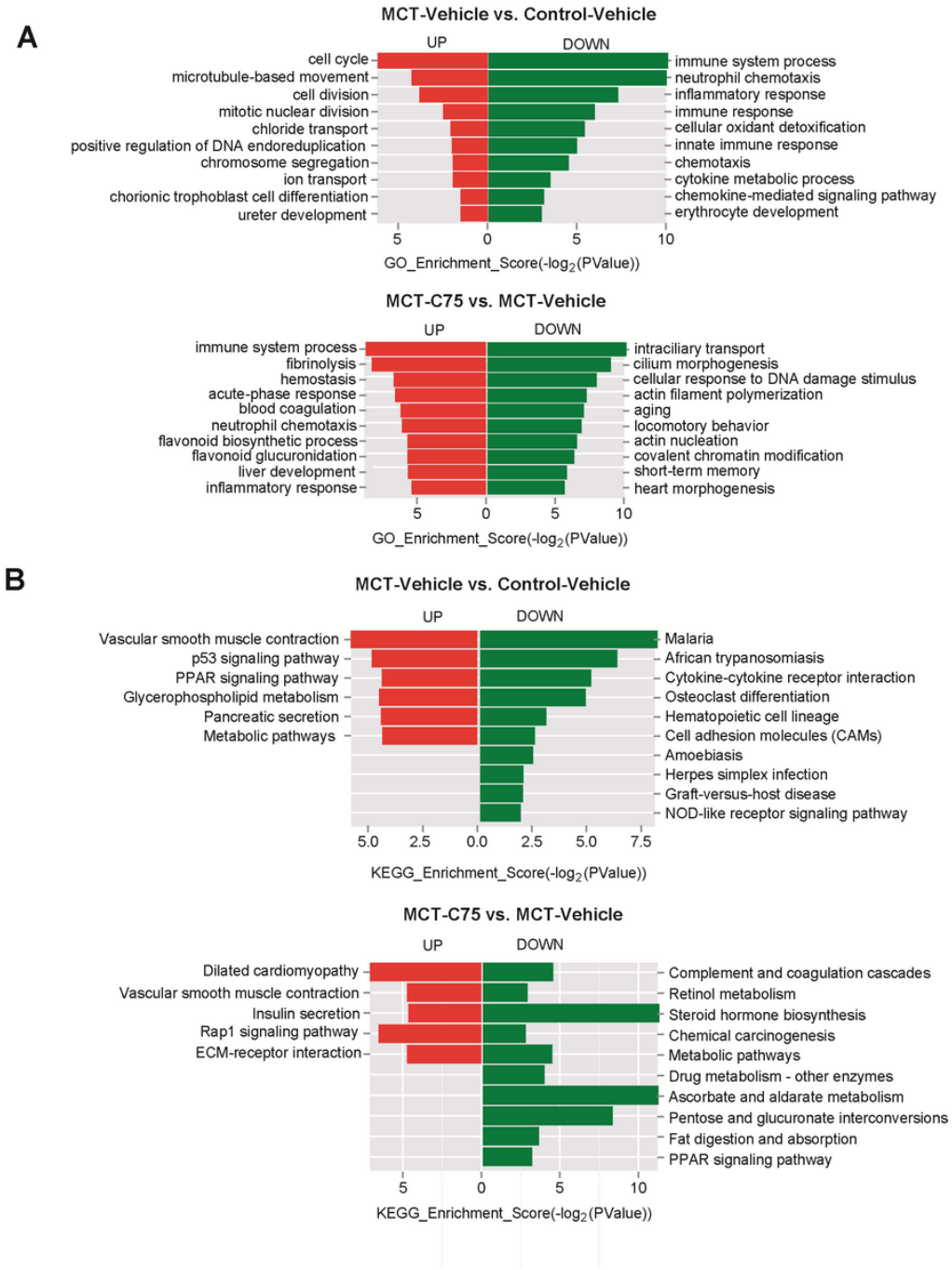

Figure 5

GO and KEGG analyses for mRNAs. A. GO analyses for mRNAs (Top 10 if enriched terms were greater than 10). B. KEGG analyses for mRNAs (Top 10 if enriched terms were greater than 10).

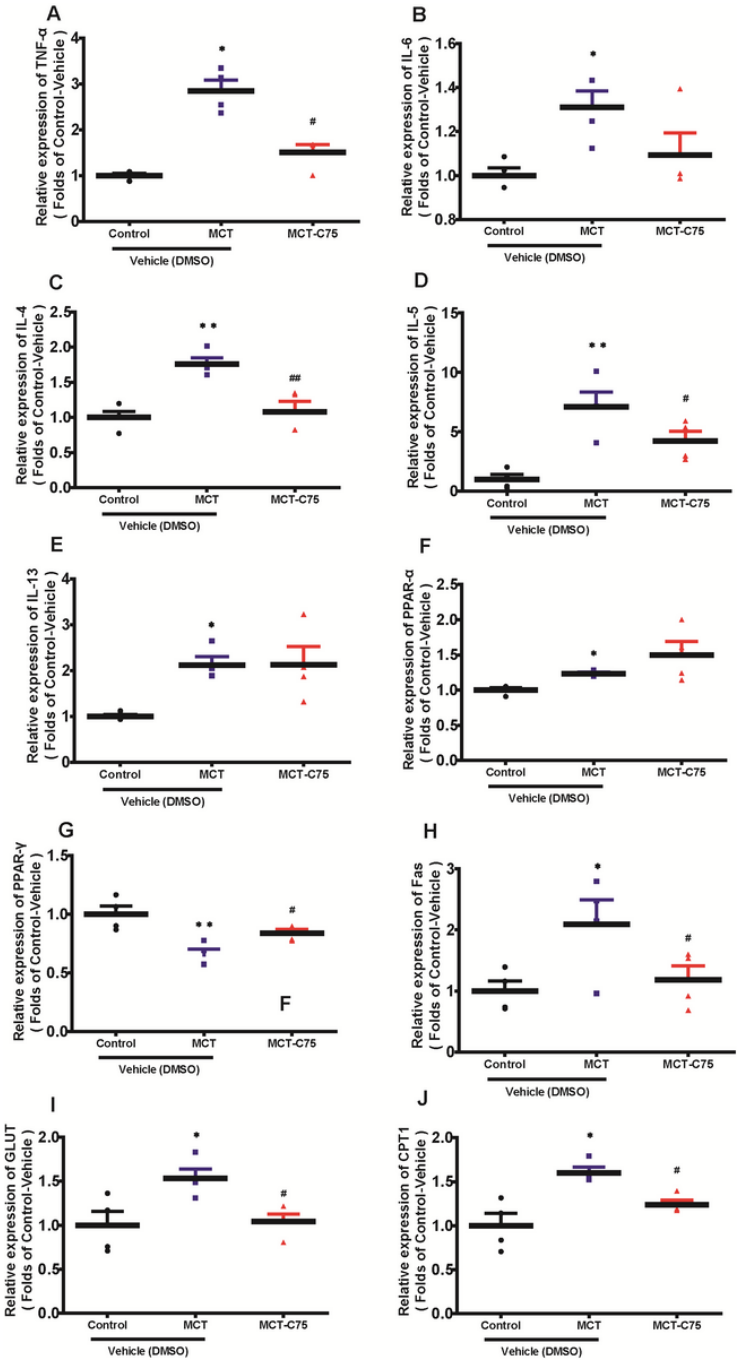

Figure 6

The protective effects of C75 on the PAH mice. A-J. The relative mRNA levels of TNF-α, IL-6, IL-4, IL-5, IL-13, PPAR-α, PPAR-γ, Fas, GLUT, and CPT1in the PAH mice. *P< 0.05.

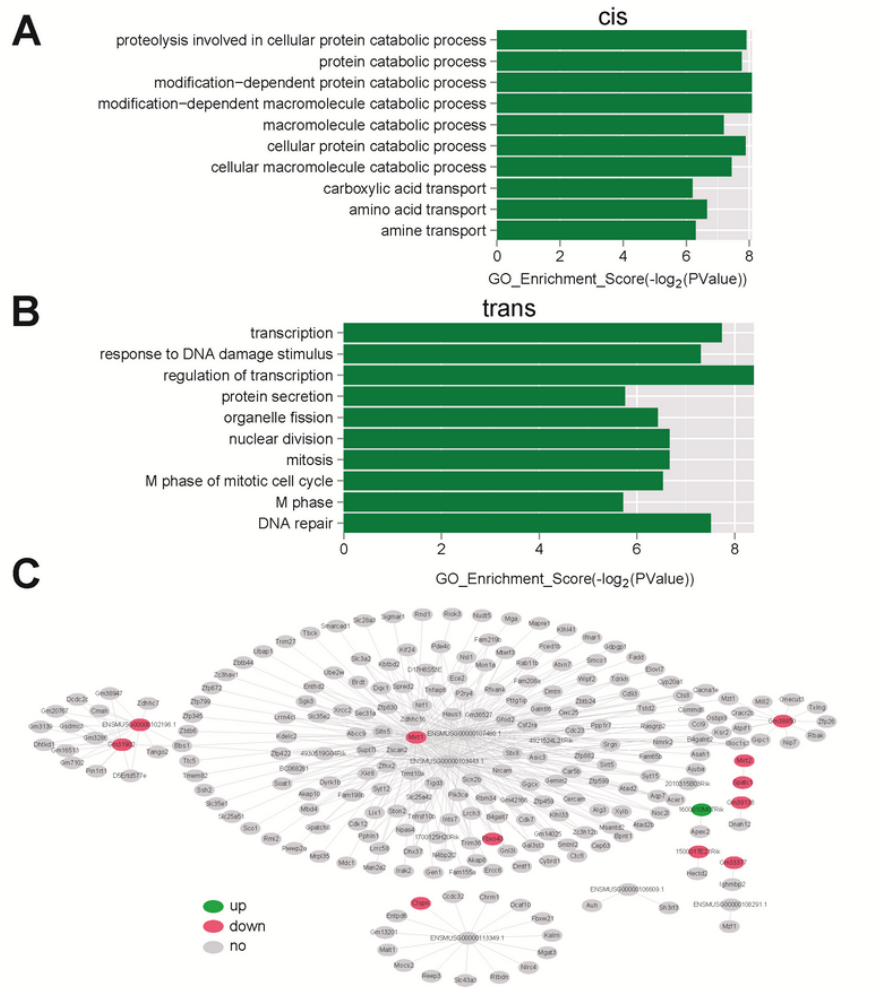

Figure 7

Target genes regulated by aberrantly expressed lncRNAs (in cis and trans) in C75-treated mice, compared with the MCT-Vehicle group. A. GO analyses of mRNAs regulated by lncRNAs in cis was forecast. B. GO analyses mRNAs regulated by lncRNAs in trans was predicted. C. LncRNA-mRNA regulatory network. D. RT-PCR validation of dysregulated lncRNAs which were identified by the HTS. E. Dysregulated lncRNAs after the HTS analysis. *$P < 0.05$.

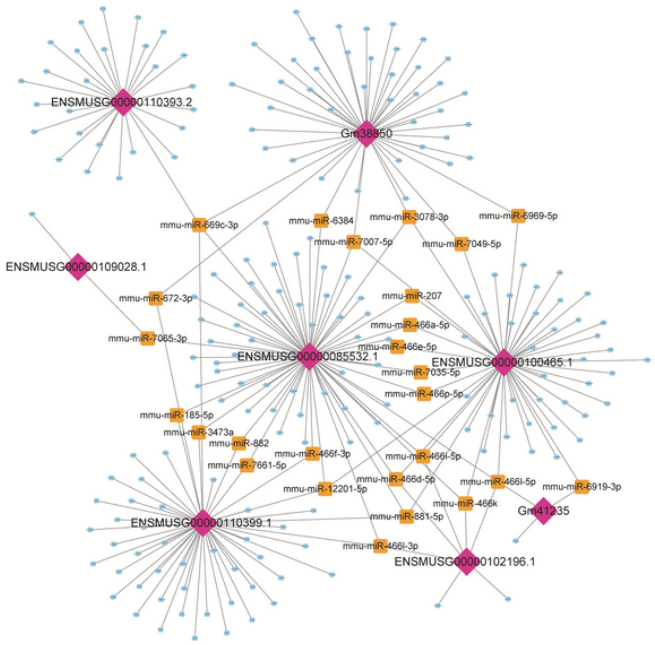

Figure 8

Regulation network of miRNA-lncRNA. Purple diamonds represent the six lncRNAs. A lncRNA with two or more than two regulation networks overlapping with those of miRNAs are marked with yellow. A lncRNA with only one regulation network overlapping with that of miRNA is indicated by blue.

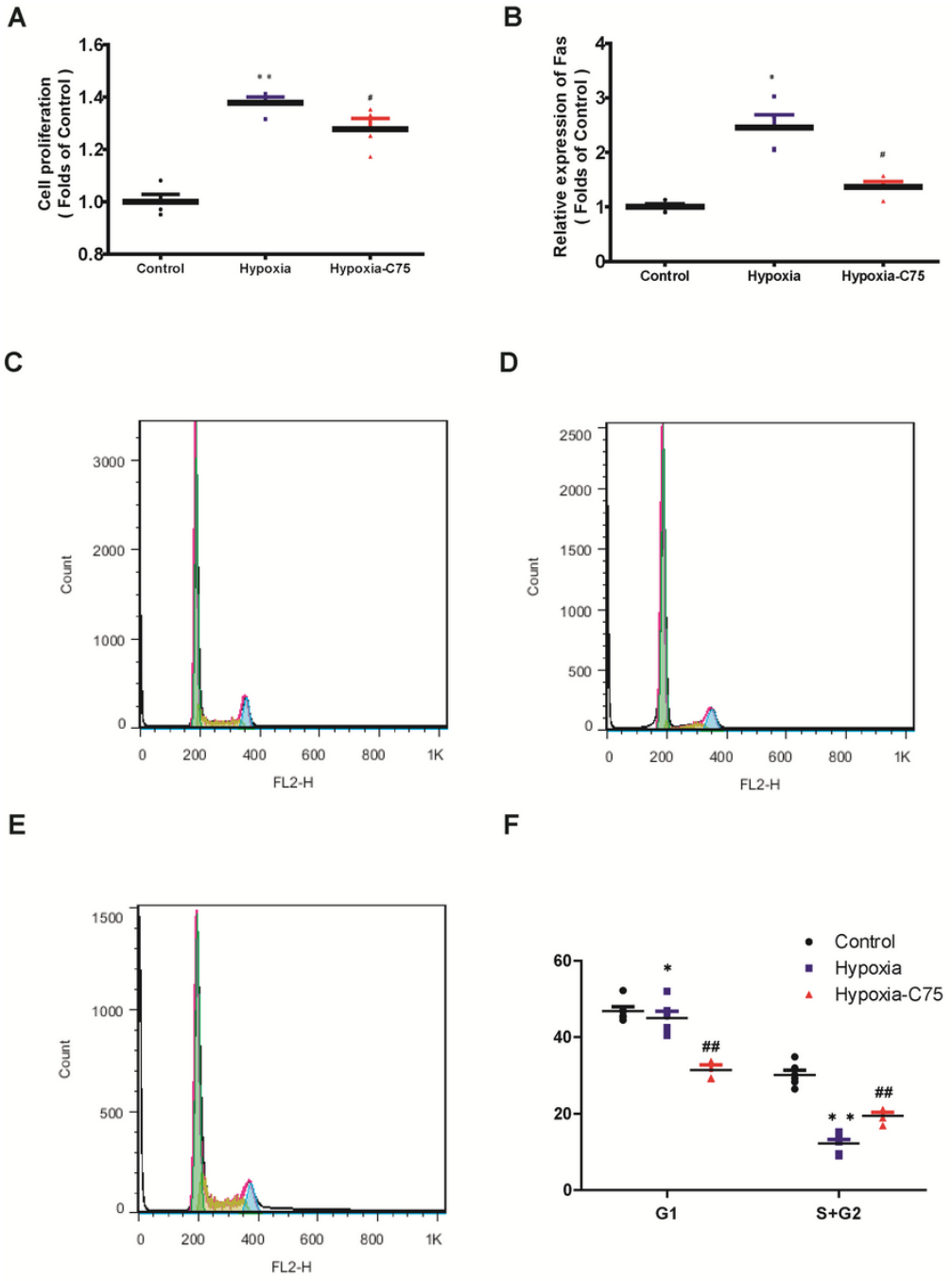

Figure 9

PASMCs cell proliferation and cell cycle after hypoxia and treatment. A. CCK-8 results of the PAMSCs. B. The relative mRNA level of Fas in the PAMSCs. C. Representative PASMCs cell cycle illustrations of the Control group. D. Representative PASMCs cell cycle illustrations of the hypoxia group. E. Representative PASMC cell cycle illustrations of the hypoxia-C75 group. F. Statistical graph of the PASMCs cell cycle. G1 means the proportion of all the PAMSCs that are in the G1 phase. S+G2 means the proportion of all the PAMSCs that are in the S and G2 phase. *P< 0.05.

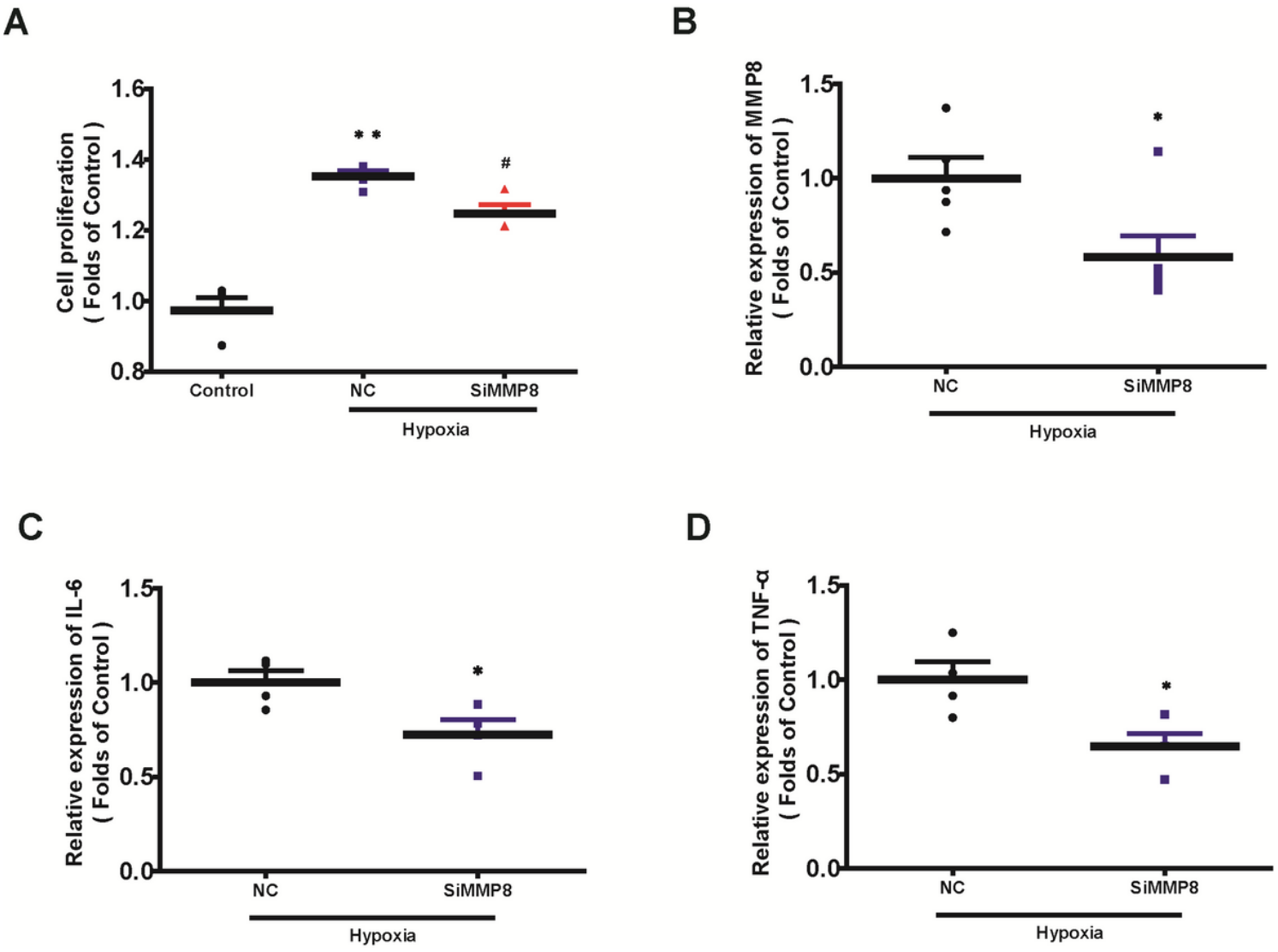

Figure 10

The protective effects of MMP8 on the PAMSCs cell proliferation and inflammation. A. The effects of MMP8 on the PAMSCs cell proliferation were detected by CCK-8 assay. B. The relative mRNA level of MMP8 in the PAMSCs cell. C-D. The relative mRNA levels of IL-6, TNF-α after MMP8 knockdown in the PAMSCs. *P< 0.05.

Supplementary Files

This is a list of supplementary files associated with this preprint. Click to download.

- Supplementarytable1.doc
- SupplementaryTable2.pdf
- SupplementaryTable3.pdf
- Supportinginformation.docx